Article

Ultrafast signatures of merocyanine overcoming steric impedance in crystalline spiropyran

Khalid M. Siddiqui [1,5] ✉, Simon F. Bittmann[1,5], Stuart A. Hayes [1,2,3], Kamil M. Krawczyk [2], Antoine Sarracini[3], Gastón Corthey [1,4], Raison Dsouza [1] & R. J. Dwayne Miller [2,3] ✉

Isomerisation through stereochemical changes and modulation in bond order conjugation are processes that occur ubiquitously in diverse chemical systems and for photochromic spirocompounds, it imparts them their functionality as phototransformable molecules. However, these transformations have been notoriously challenging to observe in crystals due to steric hindrance but are necessary ingredients for the development of reversible spiro-based crystalline devices. Here, we report the detection of spectroscopic signatures of merocyanine due to photoisomerisation within crystalline spiropyran following 266 nm excitation. Our femtosecond spectroscopy experiments reveal bond breaking, isomerisation and increase in bond order conjugation towards the formation of mercocynine on a sub-2 ps time scale. They further unveil a lifetime of several picoseconds for the initial open ring intermediate with subsequent relaxation to mercocyanine, with established back connversion pathways, which make the system highly reversible in the solid state. Supporting femtosecond electron diffraction studies suggest that lattice strain favours the return of photoproduct to the closed spiroform. Our work thus paves the way for novel ultrafast applications from spiropyran-derived compounds.

Controllable chemical reactions hold great promise for creating new dynamical photonic and optoelectronic devices[1,2]. Large structural transformations that accompany chemical metamorphosis concomitant with electronic changes naturally provide an attractive route in this direction. Much focus has recently fallen on photochromic compounds, e.g., diarylethenes[3], azobenzenes[4] and spiropyrans[5], which can switch between one or more isomeric forms via light and thermal activation making them strong candidates for photoswitching applications[6–8]. However, simply triggering the reaction is not enough,

and other factors such as switchability and photorigidity must also be considered[9–11].

An ideal photoswitching device exploiting chemical reactions must be one that can undergo an indefinite number of photocycles without degradation, display large changes in chemical and physical properties, and be triggered and ideally reversed in a controllable way. While most of these conditions can be readily met in the liquid phase[12–15], the progress has been frustrated in the solid state, which is more amenable to device applications[16]. The limitation, especially in

[1]Max Planck Institute for the Structure and Dynamics of Matter, Luruper Chaussee 149, 22761 Hamburg, Germany. [2]Department of Chemistry, University of Toronto, 80 St. George Street, Toronto, ON M5S3H6, Canada. [3]Department of Physics, University of Toronto, 60 St. George Street, Toronto, ON M5S1A7, Canada. [4]Instituto de Nanosistemas, Escuela de Bio y Nanotecnologías, Universidad Nacional de San Martín, Av. 25 de Mayo 1021, Buenos Aires, San Martín 1650, Argentina. [5]These authors contributed equally: Khalid M. Siddiqui, Simon F. Bittmann. ✉e-mail: khalid.siddiqui@phys.au.dk; dmiller@lphys2.chem.utoronto.ca
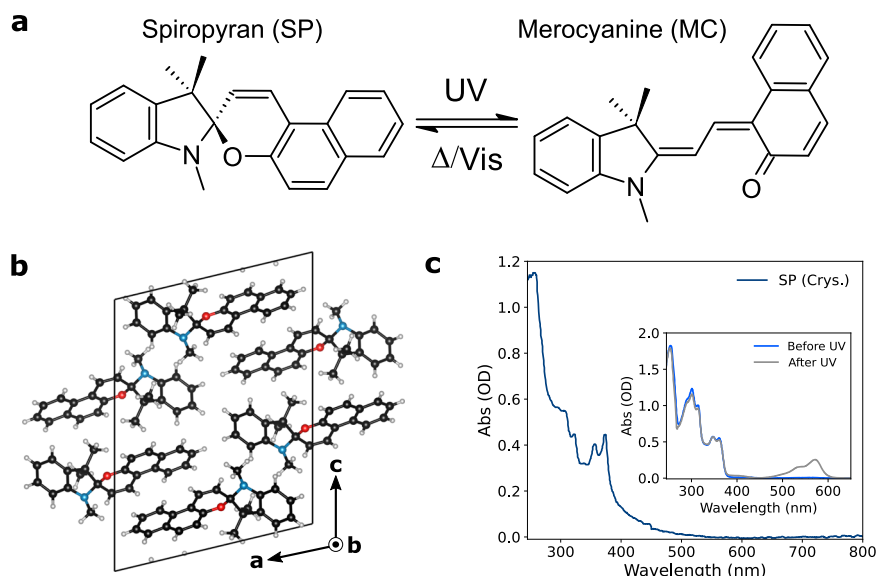
Fig. 1 | Photochromic reaction of Spiropyran. a Reaction scheme of SP to MC conversion. The forward reaction requires a UV photon whereas the back reaction occurs either thermally or via visible light activation. **b** Crystal structure of SP showing dense packing of non-planar spiropyran molecules. Red: oxygen, Black: carbon, Blue: nitrogen, White: hydrogen. **c** Measured steady-state absorption spectrum of SP crystal used in this work. The inset shows the spectra of SP dissolved in acetonitrile solvent measured before (in blue) and after (in grey) UV light irradiation. The latter results in the band in the visible range which is assigned to planar MC products. Source data is available in Zenodo repository[61].

crystals, can be related to the lack of free volume that generally prevents large changes from taking place in such sterically confined environments, and greatly limits the scope of this class of photo-induced reactions. Indeed, only a few studies have actually reported the possibility to induce reversible chemical transformation in crystals[8,17–20]. Investigations of the photochemical properties of photochromic materials and mechanisms that make them conducive or a hindrance to photoswitching applications remain an active area of research.

Spiropyrans have recently emerged as potential contenders for creating photo-activated devices on account of their remarkable tunable structural and chemical properties[21,22]. Absorption of an ultraviolet (UV) photon triggers bond-breaking and *cis–trans* isomerisation, transforming the parent spiropyran into planar merocyanine (MC, see Fig. 1a). The process has been readily observed in polymer films[23], glassy matrices and membranes[24] and in solution[14,25,26], where the mechanism involves singlet electronic states which react to form ring-opened, non-planar intermediates via a carbon–oxygen bond stretching pathway or undergo non-radiative deactivation to SP ground state via a C–N stretching coordinate on ultrafast timescales[27]. The formation of MC through the intermediate depends on the solute-solvent interaction, which can favour different isomers[25,28–30]. However, evidence of the occurrence of MC in crystals has been challenging to obtain. The latter will open new avenues for highly directional light control and further enable new studies on fundamental processes responsible for the reaction.

A few studies have hinted at the formation of MC in crystals upon UV irradiation[21,31–34], however evidence for such claims come chiefly from applying surface-sensitive tools such as diffuse-reflectance spectroscopy[35] which cannot confirm whether the reaction indeed takes place inside the bulk or only on the surface level. Static x-ray diffraction experiments have also been conducted but have remained inconclusive and reveal little about the mechanism of the reaction, including switching timescales and pathways involved[31,33].

In this article, we address the question of whether it is actually possible to induce photochromic reactions in crystals of spiropyrans using 1,3,3-Trimethylindolino-β-naphthopyrylospiran ($C_{23}H_{21}NO$, henceforth denoted SP) as a representative example from this class

of compounds and also investigate the role played by the crystal environment[36,37]. To resolve these, we employ femtosecond transient absorption (fs-TA) spectroscopy which provides sensitive bulk information on structural changes in the form of spectral signatures as a function of pump-probe delay.

Results
fs-TA spectroscopy of SP
Crystals of SP with a thickness of 250 nm were used for the fs-TA experiments. The dynamics were initiated by the UV pump pulse at an incident fluence of 2.3 mJ cm^{-2} and tracked by synchronised time-delayed visible pulses from the white light supercontinuum (see the "Methods" section). Ultrafast pump-probe studies of photochemical changes in photochromic crystals normally necessitate single-shot measurements or photoreversion schemes[3,38–40], however, remarkably this was not required in our experiments. We will return to this observation later on.

Figure 2a provides an overview of the transient changes in optical absorption, $\Delta A(\lambda, t)$, over the entire delay range covered in our study. Spectral traces at selected time delays are provided in Fig. 2b alongside kinetic plots at chosen wavelengths shown in Fig. 2c. As can be seen from these plots, right at the onset, a broad positive absorption dominates the entire 400–700 nm probe region with a maximum at 515 nm (≈45 mOD) featuring a shoulder at around 440 nm (≈20 mOD) and a broad tail of similar intensity. In the next few picoseconds, these features undergo decay as spectral evolution involving red-shift and bandwidth narrowing takes place until 10 ps, at which point the 515 nm peak has decayed by more than 70% of its initial value and a new maximum at around 570 nm emerges alongside a broad absorption with a peak at ≈470 nm. The subsequent transient data between 10 and 40 ps display a decrease of ~6–7 mOD in the 570 nm absorption as can be seen in Fig. 2a and b (see Supplementary Fig. 12 for further plots in this range). Thereafter, around 45 ps, the onset of the slow decay of the visible band is witnessed leading to a rise in optical density in the 400–450 nm region and the appearance of a negative differential signal between 450 and 550 nm over long time delays. The latter can be an indication of photobleaching of trapped products, which can lead to rapid photofatigue and eventual crystal damage[41] or it can point to
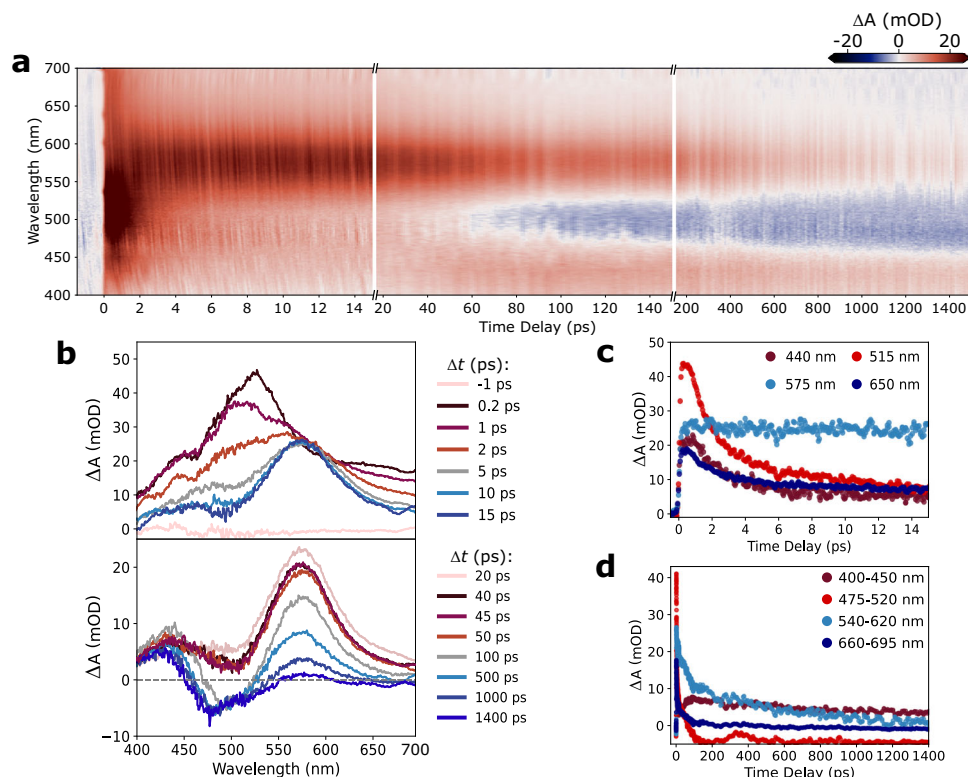
Fig. 2 | Femtosecond spectroscopy of SP. a Two-dimensional transient absorption map of SP up to 1.5 ns measured using white-light supercontinuum following 266 nm excitation. **b** Transient spectra at selected time delays showing complex dynamics of SP to MC conversion. **c** Kinetic profiles at selected wavelengths for the first 15 ps. **d** Time-evolution of the transient absorption spectra integrated over chosen wavelength range covering the full range of the delays. Slow apparent oscillations can be seen from the integrated plots. Source data is available in Zenodo repository[61].

one of the emissive photochemical deactivation processes, e.g., stimulated emission and fluorescence[42].

To rule out the origin of the negative band in our data being sample damage and/or product accumulation[40], measurements were repeated on a fresh spot on the crystal and the order of the time delay sequence was reversed, i.e. the acquisition was started at the maximum delay and the stage was stepped backward towards negative delays. The results obtained this way were found to be identical to those measured with the previous sequence on several repeats, thus assigning the negative band to a bonafide photochemical process and not sample damage or an unknown experimental artefact.

Following their emergence, the new absorption features persist for the remainder of the permissible delay range covered in our work spanning a total of 1.5 ns. The signal around selected bands was also binned along the wavelength axis and plotted as a function of pump-probe delay as shown in Fig. 2d, which revealed apparent oscillations with a period on the order of tens of picoseconds.

To disentangle the complex evolution, we reduced the TA dataset by employing global target analysis (GTA), which is a generalised form of the global fitting routine. In this case, a kinetic model was applied to fit the transient data and involves spectral species which can be cast into steps for a chemical mechanism[43-45]. The data were modelled according to a step-wise evolution of species, i.e. $A \xrightarrow{\tau_{AB}} B \xrightarrow{\tau_{BC}} C \xrightarrow{\tau_{CD}} D \xrightarrow{\tau_{DE}} E \xrightarrow{\tau_{EF}} F$ (where τ is the time constant). The results of GTA are presented in the form of species-associated difference spectra (SADS)—which denote the spectral signature of transient species—and their corresponding concentration profiles in Fig. 3. The first SADS is associated with species A created immediately following excitation. The spectral features contained here match with that of the absorption from SP in the singlet excited state, i.e. $S_1 \rightarrow S_n$ in solution (see Supplementary Fig. 9)[25]. As the excited state species A decays, it transforms into species B (second SADS) with $\tau_{AB} = 0.24$ ps. It is

known from the literature that following UV excitation, propagation of the created wave packet on the S_1 surface leads to C–O bond dissociation and formation of a non-planar, ring-opened intermediate, Z-merocynanine[22,25,34,40]. The process takes place on sub-300 fs timescales which is in good agreement with the time constant recovered for the A → B rate step.

The third SADS represents species C formed with $\tau_{BC} = 1.14$ ps with a peak at 570 nm and a shoulder around 470 nm. The peak matches well with that of the MC absorption band[25,30] in a solution of acetonitrile shown in Fig. 1c, although the 540 nm shoulder observed in a solution is not resolved here. This can be rationalised as MC is being formed in two different environments and therefore, the spectra can have differences and/or it can be due to unfavourable crystal orientation (cf. spectrum obtained for a differently oriented SP crystal shown in Supplementary Fig. 11). The spectrum is also broader and more diffuse hinting that it is likely from vibrationally hot species. In the liquid phase, photoisomerisation from ring-opened intermediate to planar MC occurs via a conical intersection (CI) and is possible due to void spaces allowing fluid motions. In solids, on the other hand, such conditions are not always available due to the steric hindrance in a crystalline environment as previously alluded. However, the resemblance between the MC band and the SADS C—which evolves slowly to SADS D (see also Supplementary Fig. 10) following some narrowing due presumably to thermal energy transfer to the phonon bath— strongly suggests the formation of incipient planar MC species in crystalline SP. Remarkably, the time scale on which planarisation takes place is only 1.14 ps. This implies that not only is MC formation possible in the bulk crystal of SP, but it occurs on ultrafast time scales. Therefore, based on these findings, the underlying mechanism of the MC formation in SP crystal can be considered to be very similar to that in solution (see later and Supplementary Note 2).
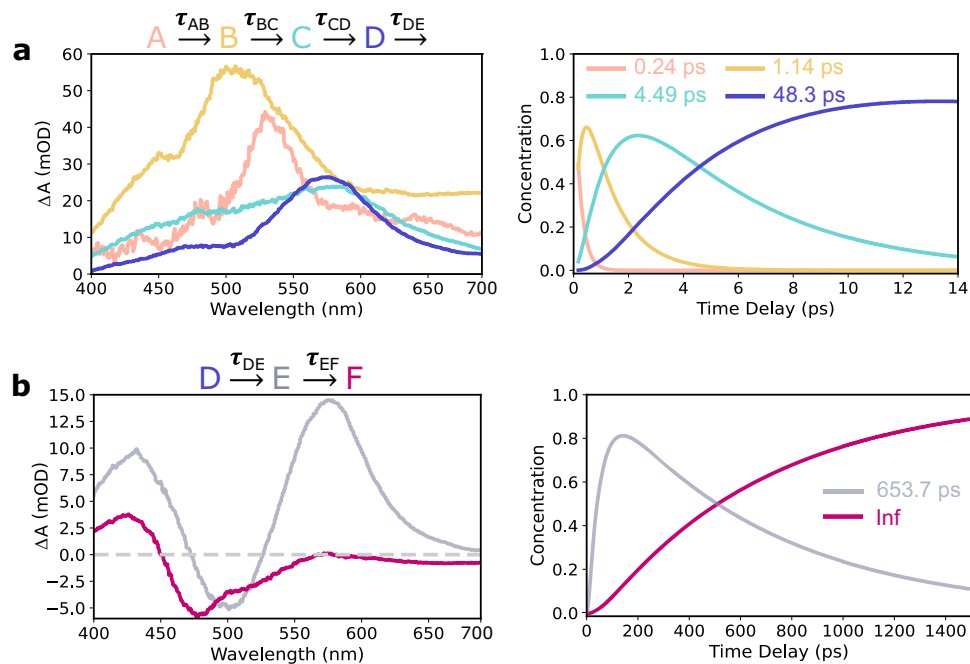
Fig. 3 | Target analysis of fs-TA data. a Species-associated difference spectra obtained from a step-wise model of the transient absorption data with corresponding percentage or concentration profiles (right panel). The evolution corresponds to the formation of MC species. **b** SADS, which describes the decay of the MC product. Source data is available in Zenodo repository[61].

However, as noted earlier, the visible band—assigned now to the planar MC product—vanishes at long time delays. This is captured in the subsequent SADS spectra, which are shown in Fig. 3b. The SADS D transforms to SADS E which features a rise in the 400–450 nm region coincident with the suppression of the MC band as well the formation of the negative band between 450–500 nm. Since a single time constant of $\tau_{DE} = 48.3$ ps describes these spectral changes, it can be concluded that they do not occur independently. This, however, complicates the interpretation as it is not obvious whether the two bands emerge from the same species or have different origins. As mentioned above, photobleaching of MC products cannot account for the negative band and since SP does not absorb in this region, neither can the photobleaching of SP. Stimulated emission is a likely explanation, but this cannot be from the MC photoproduct— whose spectrum would be Stokeshifted with respect to its ground state. This leaves the possibility of an excited state of a species with a structure close to SP (but whose precise identity remains unknown), giving rise to the emergent signals or some other effect (see Supplementary Note 4). While this is not the main focus of the present work, this aspect could be investigated more closely in future studies using more advanced methods, which can disentangle the decay pathways, e.g. two-dimensional spectroscopy[29] to resolve this issue.

The time constant, τ_{EF} of 653.7 ps for the E → F rate step establishes the slow decay of merocyanine products. Normally, it would be difficult to comprehend this observation as it defies the general expectation that any MC formed will become trapped and remain so under spatial confinement[31,46,47]. However, a conjecture could be made in which MC product formation leads to transient distortion of the crystal lattice, resulting in strain, which leaves the system in an energetically unfavourable state. As the surrounding lattice molecules are not as free to move as they would be in solution to stabilise the MC photoproduct state, this steric constraint on lattice relaxation reduces the barrier for the back reaction in single crystals in comparison to the solution phase[24]. The built-up stress also causes strain wave propagation manifesting as the apparent oscillations on several tens of picoseconds timescales.

Transient strain formation
We have further examined the plausibility of the hypothesis that strain is acting on the system with supporting femtosecond electron diffraction (FED) experiments which can provide direct information about the crystalline lattice by recording the changes in diffraction intensity and the latter can be related to the changes in the atomic positions within the unit cell.[48–51] Pump-probe diffraction patterns of 150 nm-thick SP crystal film were measured for up to 5 ps time delay. The results of these measurements are presented in Fig. 4 and show changes in the diffraction pattern averaged over all measured time delays following photoexcitation with 266 nm at 1.3 mJ cm⁻². A butterfly pattern—in which the central part shows suppression of Bragg peak intensity whereas the wings display a rise—as observed in Fig. 4b for the labelled diffraction orders in Fig. 4a, of which one is selected for closer examination in Fig. 4c. These changes reflect lattice strain caused by distortions of the unit cell leading to a distribution of sizes and therefore broader diffraction peaks[52]. A simplified model involving Gaussian profiles can be used to illustrate the effect of induced broadening (Fig. 4d): the Pump_ON peak is 40% broader than the initial width (Pump_OFF), and the difference between Pump_ON and Pump_OFF yields a peak profile that matches the one observed in the experiment giving credence to our prediction that lattice strain is at play. We discount the possibility that other effects such as laser heating of the lattice contribute significantly as that would give rise to a qualitatively different diffraction signal: it would manifest in the form of the Debye-Waller effect in which the increase of lattice temperature leads to the drop of Bragg peak intensity which scales as q^2, where q is the scattering vector[53–56].

It should be mentioned that the early onset of strain generation within 5 ps post-excitation convolved with the formation of the intermediate and MC product hinders unambiguous determination of their structures from FED. Conversely, strain relaxation facilitates the eventual return of MC back to the spiro form over long time scales, meaning that the system is exceptionally reversible, surviving several hundred thousand photocycles, as found in this study. To put these numbers into context, a crystal of spirooxazine with a very similar chemical composition (has just one CH_2 moiety on the pyran ring replaced with an NH group) was investigated previously using fs-TA
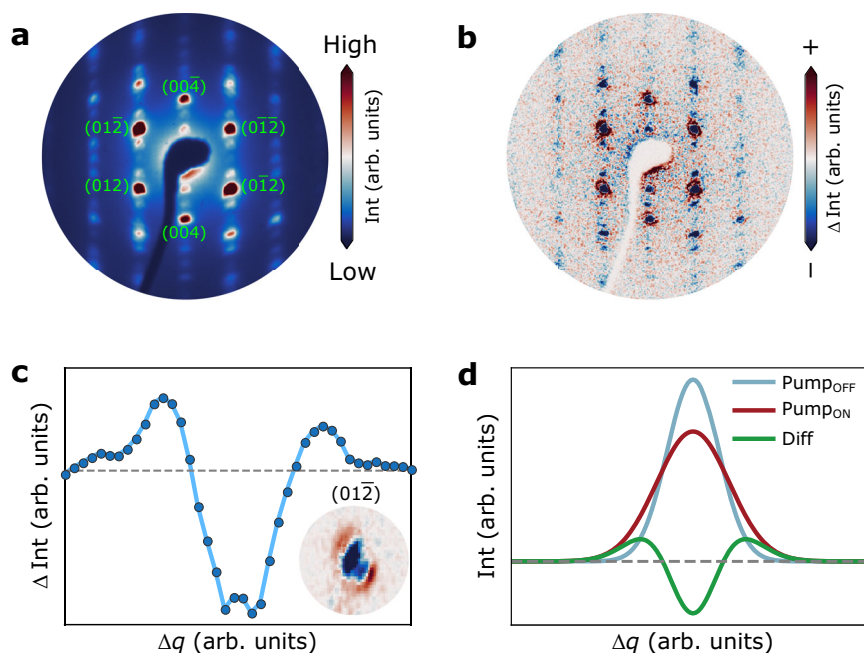
Fig. 4 | Femtosecond electron diffraction of crystalline SP. a Static diffraction pattern of 150 nm crystal film of SP looking down [100] axis. **b** Averaged difference pattern obtained following 266 nm excitation. **c** Difference intensity plot of $(01\bar{2})$ peak. Inset: Zoomed-in view of the difference map of peak $(01\bar{2})$. **d** Illustration of the effect of broadening on diffraction peaks due to lattice strain. Source data is available in Zenodo repository[61].
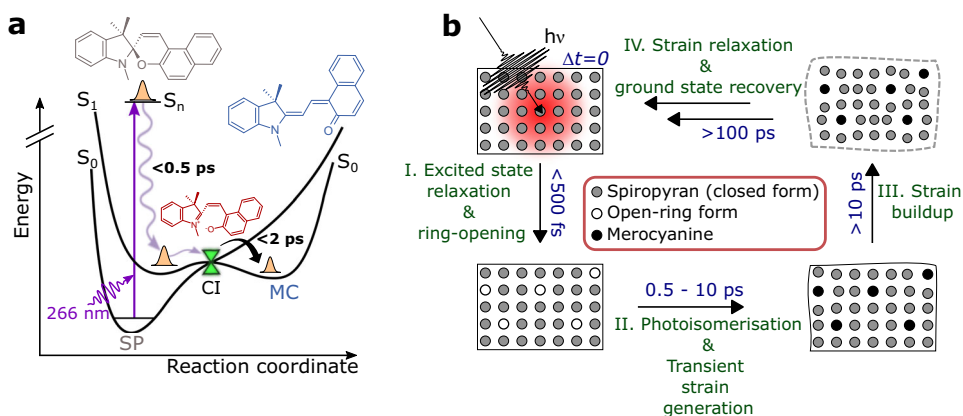
Fig. 5 | Proposed stages of the photoinduced dynamics. a SP to MC: Ultraviolet laser excitation creates a propagating wave packet along the C–O bond stretching coordinate leading to C–O bond breaking and ring-opening followed by hybridisation and isomerisation to planar MC. Singlet electronic states are denoted by S_j where $j = 0, 1, \ldots, N$. CI conical intersection (**b**) Sketch depicting the buildup of lattice strain due to SP to MC switching and eventual relaxation to SP.

spectroscopy and FED[57] and was found to rapidly lose long-range order due to permanent product accumulation from fewer than a hundred UV laser shots and required novel photoreversion schemes to prevent sample damage[40]. In the latter scenario, under fully reversible conditions, UV excitation was found to only create the ring-opened, non-planar intermediate that remained trapped in crystal for several hundred picoseconds without any evidence of planar MC formation. In contrast, in the present work, not only bond breaking followed by isomerisation and increased double bond conjugation occurred, but assisted by strain, these large amplitude motions were reversed on relatively fast time scales. As a consequence, over 100,000 photochemical cycles could be attained bereft of any noticeable sample degradation and without the need for inducing any photoreversion between pump laser shots.

Discussion

Ultrafast photoisomerisation and subsequent relaxation of the MC form have been realised in bulk single crystals of spiropyran in this work. The proposed events are summarised in Fig. 5. The timescale of SP-MC conversion is ~1–2 ps, very similar to that in solution suggesting that a sterically hindered crystalline environment is not creating a significant barrier relative to the forces directing the chemistry leading to bond breaking coupled to isomerisation and changes in double bond conjugation. The formed MC product is long-lived but not permanent over a nanosecond timescale, resulting in a very high number of photocycles (>10^5) that were achieved in SP crystals, which bodes very well for their prospects towards ultrafast photoswitching applications. Thus, while SP is not photochromic in the solid state in the conventional sense, our results suggest that the lifetime of the MC is long enough to furnish this property transiently by the addition of a secondary (delayed) laser pulse tuned to the maximum of the MC absorption band to provide photoswitching properties on fast timescales.

Furthermore, our fs-TA and FED measurements indicate that inherent steric constraints within the solid state lead to strain that, in turn, creates forces opposing the formation of the fully relaxed

product states. This insight provides a means to engineer lattice strain as a tool for controlling the overall reaction pathways with spiro-based devices forming a model system to explore this concept[58]. Thus, our work could have a sizeable impact on efforts to enable solid state photochromism in challenging photolabile and sterically congested systems. In particular, the role of molecule–lattice interaction and strain revealed in this study could be critical for harvesting the complete system response on ultrafast timescales which would unlock the full potential of photochromics from spiropyran-derived compounds and beyond.

Finally, further studies are warranted to fully capture the mechanism behind SP-MC interconversion using both theoretical and experimental approaches, especially in the time domain to clarify the identity of the photo-generated isomer and the select reaction modes that lead to the specific stereochemistry driven by the increased double bond conjugation. This selective mode coupling and possible photodark intermediates will fully resolve the driving forces for this eminent class of chemical reactions. To this end, the stability of SP crystals under photoexcitation enables unlimited sampling of the reaction dynamics to provide an ideal model system to explore these details at the highest possible spatiotemporal resolution.

Methods

Transient absorption spectroscopy

Optical experiments were performed using a home-built transient absorption setup at room temperature[40]. The fundamental output of a mode-locked, Ti:Sapph oscillator and regenerative amplifier system delivering 35 fs FWHM, 800 nm pulses at 1 kHz was divided using a 90:10 beamsplitter to create pump and probe arms. In the probe arm, ≈2 μJ of 800 nm light was focused onto a 200 μm window of a cuvette containing water that generated a white light supercontinuum from 380 to 900 nm. A shortpass cut-off filter at 700 nm was placed in the beam path to remove the fundamental beam from the white light. UV light of 266 nm wavelength and ≈100 fs FWHM pulse duration was generated in the pump arm using a set of barium beta-borate (BBO) and calcite crystals and focused onto the crystalline sample using a concave mirror ($f = 200$ mm). The repetition rate of the probe was set at 1 kHz and the pump was run at 20.83 Hz to ensure ample time for sample relaxation between laser shots. Finally, the data acquisition was broken down into stages spanning three different time ranges, namely 1–15 ps (50 fs steps), 15–150 ps (1 ps step size) and 150–1400 ps (5 ps steps). The delay stage was stepped linearly in the following order: forward → backward → forward, and the data was averaged. A complete scan sequence took between 30 and 90 min to finish depending on the amount of averaging per time point (up to 100 pump-probe cycles were averaged).

SP samples

The SP powder was purchased from TCI Chemicals, Japan and used without further purification. The sample crystals were grown in the dark from a saturated solution of the compound in Ethyl Acetate. Crystals of SP were then cleaved using an ultramicrotome to the desired thickness of 150–250 nm for the experiments and mounted on a 1 mm-thick fused silica disc. All experiments were performed at room temperature with the samples inside a cryostat that was thoroughly purged with dry nitrogen gas. No sample translation was needed.

Femtosecond electron diffraction

Femtosecond electron diffraction (FED) experiments were carried out using a home-built setup based on a DC electron gun with radio frequency compression[59,60]. The driving laser was a Ti:Sapph-based amplifier whose output was frequency-tripled to create 266 nm light, used for both photoexcitation and generation of electron bunches via photoemission from a gold photocathode. Each bunch was accelerated to 95 keV and contained ~10^5 electrons. SP samples used for FED were microtomed to 150 nm and mounted as free-standing films onto a standard TEM Cu-mesh from Ted Pella. The experiment was conducted under a high vacuum ($P \le 10^{-7}$ mbar) with a sample temperature of 270 K. The repetition rate for the experiments was 25 Hz, and at each time delay, a sequence of pump ON and pump OFF images were recorded.

Data availability

Data that support the findings of this study are deposited at the Zenodo repository[61] under the accession code https://doi.org/10.5281/zenodo.14022139. Source data are provided with this paper.

References

1. Klajn, R. Spiropyran-based dynamic materials. *Chem. Soc. Rev.* **43**, 143–184 (2014).
2. Andréasson, J & Pischel, U. *Molecular Photoswitches for Information Processing: From Simple to Complex* Vol. 33, 785–809 (John Wiley & Sons, Ltd, 2022).
3. Jean-Ruel, H. et al. Femtosecond dynamics of the ring closing process of diarylethene: a case study of electrocyclic reactions in photochromic single crystals. *J. Phys. Chem. A* **115**, 13158–13168 (2011).
4. Bandara, H. M. D. & Burdette, S. C. Photoisomerization in different classes of azobenzene. *Chem. Soc. Rev.* **41**, 1809–1825 (2012).
5. Fleming, C. et al. Shining new light on the spiropyran photoswitch: a photocage decides between *cis–trans* or spiro-merocyanine isomerization. *J. Am. Chem. Soc.* **140**, 14069–14072 (2018).
6. Irie, M. Photochromism: memories and switches. *Chem. Rev.* **100**, 1683–1684 (2000).
7. Natali, M. et al. Molecular switches as photocontrollable "smart" receptors. *Chem. Soc. Rev.* **16**, 4010–4029 (2012).
8. Krawczyk, K. M. et al. Illuminating the photoisomerization of a modified azobenzene single crystal by femtosecond absorption spectroscopy. *Can. J. Chem.* **97**, 488–495 (2019).
9. Irie, M. Photochromism of diarylethene molecules and crystals. *Proc. Jpn. Acad. Ser. B* **86**, 472–483 (2010).
10. Goulet-Hanssens, A. et al. Enlightening materials with photoswitches. *Adv. Mater.* **32**, 1905966 (2020).
11. Lameijer, L. et al. General principles for the design of visible-light-responsive photoswitches: tetra-*ortho*-chloro-azobenzenes. *Angew. Chem. Int. Ed.* **59**, 21663–21670 (2020).
12. Antipin, S. et al. Femtosecond transient absorption spectroscopy of nonsubstituted photochromic spirocompounds. *Chem. Phys. Lett.* **331**, 378–386 (2020).
13. Tamai, N. & Masuhara, H. Femtosecond transient absorption spectroscopy of a spirooxazine photochromic reaction. *Chem. Phys. Lett.* **19**, 189–194 (1992).
14. Zhang, J. Z. et al. Ultrafast studies of photochromic spiropyrans in solution. *JACS* **114**, 10921–10927 (1992).
15. Tian, W. & Tian, J. A. An insight into the solvent effect on photo-, solvato-chromism of spiropyran through the perspective of intermolecular interactions. *Dyes Pigment.* **105**, 66–74 (2014).
16. Ru, Y. et al. Recent progress of photochromic materials towards photocontrollable devices. *Mater. Chem. Front.* **5**, 7737–7758 (2021).
17. Irie, M. et al. Photochromism of diarylethene molecules and crystals: memories, switches, and actuators. *Chem. Rev.* **114**, 12174–12277 (2014).
18. Kobatake, S. et al. Rapid and reversible shape changes of molecular crystals on photoirradiation. *Nature* **446**, 778–781 (2007).
19. Xian, R. et al. Coherent ultrafast lattice-directed reaction dynamics of triiodide anion photodissociation. *Nat. Chem.* **9**, 516–522 (2017).
20. Cole, J. M. et al. Light-Induced macroscopic peeling of single crystal driven by photoisomeric nano-optical switching. *Chem. Mater.* **31**, 4927–4935 (2019).

21. Zhang, L. Solid-state spiropyrans exhibiting photochromic properties based on molecular flexibility. *Mater. Chem. Front.* **5**, 3119–3124 (2021).

22. Kortekaas, L. & Browne, W. R. The evolution of spiropyran: fundamentals and progress of an extraordinarily versatile photochrome. *Chem. Soc. Rev.* **48**, 3406–3424 (2019).

23. Tork, A. et al. Photochromic behavior of spiropyran in polymer matrices. *Appl. Opt.* **40**, 1180 (2001).

24. Janissen, R. & Filonenko, G. A. Mechanochemistry of spiropyran under internal stresses of a glassy polymer. *J. Am. Chem. Soc.* **144**, 23198–23204 (2013).

25. Bittmann, S. F. et al. Ultrafast ring-opening and solvent-dependent product relaxation of photochromic spironaphthopyran. *Phys. Chem. Chem. Phys.* **21**, 18119–18127 (2019).

26. Krysanov, S. A. & Alfimov, M. V. Ultrafast formation of transients in spiropyran photochromism. *Chem. Phys. Lett.* **91**, 77–80 (1982).

27. Rosaria di Nunzio, M. et al. Ultrafast excited-state dynamics in some spirooxazines and chromenes. Evidence for a dual relaxation pathway. *Photochem. Photobiol. Sci.* **9**, 1391–1399 (2010).

28. Rini, M. et al. Ultrafast UV-mid-IR Investigation of the ring opening reaction of a photochromic spiropyran. *J. Am. Chem. Soc.* **125**, 3028–3034 (2003).

29. Buback, J. et al. Ultrafast bidirectional photoswitching of a spiropyran. *J. Am. Chem. Soc.* **132**, 16510–16519 (2010).

30. Kohl-Landgraf, J. et al. Ultrafast dynamics of a spiropyran in water. *J. Am. Chem. Soc.* **134**, 14070–14077 (2012).

31. Harada, J., Kawazoe, Y. & gawa, K. Photochromism of spiropyrans and spirooxazines in the solid state: low temperature enhances photocoloration. *Chem. Commun.* **46**, 2593–2595 (2010).

32. Lukyanov, B. S. & Yoffe, A. Solid state photochromism of spiropyrans. *Adv. Phys.* **7**, 17–22 (2005).

33. Wu, Z. et al. Photochromism of neutral spiropyran in the crystalline state at room temperature. *J. Mater. Chem. C* **9**, 6290–6296 (2021).

34. Suzuki, M., Tsuyoshi, A. & Masuhara, H. Photochromic reactions of crystalline spiropyrans and spirooxazines induced by intense femtosecond laser excitation. *Phys. Chem. Chem. Phys.* **4**, 185–192 (2022).

35. Suzuki, M., Tsuyoshi, A. & Masuhara, H. Cooperative photochemical reaction mechanism of femtosecond laser-induced photocoloration in spirooxazine microcrystals. *Chem. Phys. Chem.* **6**, 2396–2403 (2005).

36. Day, J. H. Thermochromism. *Chem. Rev.* **63**, 65–80 (1963).

37. Mustafa, A. The chemistry of spiropyrans. *Chem. Rev.* **43**, 509–523 (1948).

38. Poulin, P. R. & Nelson, K. A. Irreversible organic crystalline chemistry monitored in real time. *Science* **313**, 1756–1760 (2006).

39. Jean-Ruel, H. et al. Ring-closing reaction in diarylethene captured by femtosecond electron crystallography. *J. Phys. Chem. A.* **117**, 15894–15902 (2013).

40. Siddiqui, K. M. et al. Synchronised photoreversion of spirooxazine ring opening in thin crystals to uncover ultrafast dynamics. *CrystEngComm* **18**, 7212–7216 (2016).

41. Herder, M. et al. Improving the fatigue resistance of diarylethene switches. *J. Am. Chem. Soc.* **7**, 2738–2747 (2015).

42. Berera, R., van Grondelle, R. & Kennis, J. T. M. Ultrafast transient absorption spectroscopy: principles and application to photosynthetic systems. *Photosynth Res.* **101**, 105–118 (2009).

43. Bittmann, S. F. *Isomerization Dynamics of Photochromic Compounds in Solution and Single Crystals*. PhD Thesis, Universität Hamburg (2022).

44. van Stokkum, I. H. M., Larsen, D. S. & van Stokkum, I. H. M. Global analysis, multiway data, photoactive yellow protein, spectro-temporal model, target analysis, time-resolved spectroscopy. *BBA —Bioenergetic* **1657**, 82–104 (2004).

45. Ruckebusch, C. et al. Comprehensive data analysis of femtosecond transient absorption spectra: a review. *J. Photochem. Photobiol. C* **13**, 1–27 (2012).

46. Seiler, V. K. et al. Acidochromic spiropyran–merocyanine stabilisation in the solid state. *CrystEngComm* **20**, 3318–3327 (2018).

47. Wu, Z. et al. Tetraphenylethene-induced free volumes for the isomerization of spiropyran toward multifunctional materials in the solid state. *ACS Appl. Mater. Interfaces* **10**, 30879–30886 (2018).

48. Miller, R. J. D. Femtosecond crystallography with ultrabright electrons and X-rays: capturing chemistry in action. *Science* **343**, 1108–1116 (2014).

49. Ishikawa, T. et al. Direct observation of collective modes coupled to molecular orbital–driven charge transfer. *Science* **350**, 1501–1505 (2015).

50. Filippetto, D. et al. Ultrafast electron diffraction: visualizing dynamic states of matter. *Rev. Mod. Phys.* **94**, 045004 (2022).

51. Siddiqui, K. M. et al. Relativistic ultrafast electron diffraction at high repetition rates. *Struct. Dyn.* **10**, 4453–4459 (2023).

52. Luo, D. et al. Ultrafast optomechanical strain in layered GeS. *Nano Lett.* **23**, 2287–2294 (2023).

53. Tinnemann, V. et al. Ultrafast electron diffraction from a Bi(111) surface: Impulsive lattice excitation and Debye–Waller analysis at large momentum transfer. *Struct. Dyn.* **6**, 035101 (2019).

54. VandenBussche, E. J. & Flannigan, D. J. Sources of error in Debye–Waller-effect measurements relevant to studies of photo-induced structural dynamics. *Ultramicroscopy* **196**, 111–120 (2019).

55. Krawczyk, K. M. et al. Anisotropic, nonthermal lattice disordering observed in photoexcited PbS quantum dots. *J. Phys. Chem. C* **125**, 22120–22132 (2021).

56. Durham, D. B. et al. Accurate quantification of lattice temperature dynamics from ultrafast electron diffraction of single-crystal films using dynamical scattering simulations. *Struct. Dyn.* **9**, 064302 (2022).

57. Siddiqui, K. M. *Investigating Photoinduced Phenomena in Molecular Crystals with Prospects for Atomically-resolved Dynamics*. PhD Thesis, University of Leeds (2017).

58. Loan, T., Santra, M. & Bradley, M. Novel class of photochromic molecules exhibiting photo-switching in the solid state. *Front. Chem.* **11**, 1205452 (2023).

59. Gao, M. et al. Mapping molecular motions leading to charge delocalization with ultrabright electrons. *Nature* **496**, 343–346 (2013).

60. Liu, L. C. et al. Ultrafast electron diffraction study of single-crystal (EDO-TTF)$_2$SbF$_6$: Counterion effect and dimensionality reduction. *Chem. Phys. Lett.* **683**, 160–165 (2017).

61. Siddiqui, K. M. et al. Dataset for: ultrafast signatures of merocyanine overcoming steric impedance in crystalline spyiropyran. *Zenodo* https://doi.org/10.5281/zenodo.14022139 (2024).

Author contributions

K.M.S. and R.J.D.M. conceived the experiment. G.C. designed, constructed, and programmed the fs-TA spectroscopy setup, which was upgraded by K.M.S. and S.F.B. K.M.S. and S.F.B. performed the fs-TA experiments and sample preparation with assistance from S.A.H. S.F.B., S.A.H., K.M.K. and A.S. carried out the FED experiments. S.F.B., K.M.S., and S.A.H. analysed the data with theoretical assistance from R.D. R.J.D.M. supervised the project. All authors contributed to data

interpretations and discussions. K.M.S. wrote the manuscript with input from all authors.

Competing interests

The authors declare no competing interests.

Additional information

Supplementary information The online version contains supplementary material available at https://doi.org/10.1038/s41467-024-54992-7.

Correspondence and requests for materials should be addressed to Khalid M. Siddiqui or R. J. Dwayne Miller.

Peer review information *Nature Communications* thanks Dongsheng Wang and the other, anonymous, reviewer(s) for their contribution to the peer review of this work. A peer review file is available.

Reprints and permissions information is available at http://www.nature.com/reprints